INTERNATIONAL JOURNAL FOR NUMERICAL METHODS IN ENGINEERING
Int. J. Numer. Meth. Engng 2005; **63**:1961–1974
Published online 11 May 2005 in Wiley InterScience (www.interscience.wiley.com). DOI: 10.1002/nme.1352

Lower bound limit analysis with adaptive remeshing

Andrei V. Lyamin*, †, Scott W. Sloan, Kristian Krabbenhøft and Mohammed Hjiaj

Geotechnical Research Group, Civil, Surveying and Environmental Engineering, School of Engineering, The University of Newcastle, University Drive, Callaghan, NSW 2308, Australia

SUMMARY

The objective of this work is to present an adaptive remeshing procedure for lower bound limit analysis with application to soil mechanics. Unlike conventional finite element meshes, a lower bound grid incorporates statically admissible stress discontinuities between adjacent elements. These discontinuities permit large stress jumps over an infinitesimal distance and reduce the number of elements needed to predict the collapse load accurately. In general, the role of the discontinuities is crucial as their arrangement and distribution has a dramatic influence on the accuracy of the lower bound solution (*Limit Analysis and Soil Plasticity*, 1975). To ensure that the discontinuities are positioned in an optimal manner requires an error estimator and mesh adaptation strategy which accounts for the presence of stress singularities in the computed stress field.

Recently, Borges *et al*. (*Int. J. Solids Struct*. 2001; **38**:1707–1720) presented an anisotropic mesh adaptation strategy for a mixed limit analysis formulation which used a directional error estimator. In the present work, this strategy has been tailored to suit a discontinuous lower bound formulation which employs the stresses and body forces as primary unknowns. The adapted mesh has a maximum density of discontinuities in the direction of the maximum rate of change in the stress field. For problems involving strong stress singularities in the boundary conditions (e.g. a strip footing), the automatic generation of discontinuity fans, centred on the singular points, has been implemented.

The efficiency of the proposed technique is demonstrated by analysis of two classical soil mechanics problems; namely the bearing capacity of a rigid strip footing and the collapse of a vertical cut.

KEY WORDS: lower bound; limit analysis; finite elements; error estimation; adaptivity

1. INTRODUCTION

Over the last decade, adaptive finite element analysis has become common practice in computational mechanics [1–5] with new applications constantly emerging [6, 7]. The extension of these procedures to lower bound limit analysis is the objective of this study.

*Correspondence to: Andrei V. Lyamin, Geotechnical Research Group, Civil, Surveying and Environmental Engineering, School of Engineering, The University of Newcastle, University Drive, Callaghan, NSW 2308, Australia.
†E-mail: andrei.lyamin@newcastle.edu.au

Received 11 June 2004
Revised 26 September 2004
Accepted 27 September 2004

A critical aspect of any adaptive meshing process is the estimation of the discretization error present in a given finite element solution. Since *a priori* error estimates are not available in limit analysis [8], useful error estimation must employ *a posteriori* techniques to predict the overall discretization error and extract a meaningful mesh refinement indicator. Recently, Borges *et al*. [8] presented an anisotropic adaptive strategy for a mixed limit analysis formulation which focused on the use of a directional error estimator. The plastic multiplier field was taken as the control variable and the approach was shown to be able to localize the mesh on the zones of intense plastic deformation, align the stretched elements along the shear bands and, finally, significantly improve the numerical evaluation of the collapse loads. Although the lower bound formulation deals directly only with stress fields, it is still possible to obtain quasi velocities and plastic multipliers from the dual solution. Therefore we will base this study on the approach described by Borges *et al*. [8], taking into account the specific features of lower bound limit analysis that will be briefly described in the next section.

In any adaptive finite element procedure, the automatic mesh generator is a key component. Very little work, however, has been done on automatic mesh generation methods for discontinuous lower bound methods [9]. Such methods must include the ability to construct 'fan' zones that are centred on singularities in the stress boundary conditions. These fans of statically admissible stress discontinuities allow a rapid transition of the stresses in a circumferential direction about the singular point. For many practical applications, the highest lower bounds are obtained for fans with the greatest number of discontinuities [10], as these permit the largest rotation of the principal stresses. It will be shown that, with appropriate modification, the advancing front mesh generator proposed by Peraire *et al*. [1] can be used to generate lower bound limit meshes that incorporate stress fans.

2. DISCRETE FORMULATION OF LOWER BOUND THEOREM

Consider a domain Ω with boundary Γ, as shown in Figure 1. Let $\mathbf{t}$ and $\mathbf{q}$ denote, respectively, a set of fixed tractions acting on part of the boundary Γ_t and a set of unknown tractions acting on part of the boundary Γ_q. Similarly, let $\mathbf{g}$ and $\mathbf{h}$ be a system of fixed and unknown body forces, respectively, which act on the volume Ω. Under these conditions, the objective of a lower bound calculation is to find a stress distribution which satisfies equilibrium throughout Ω,

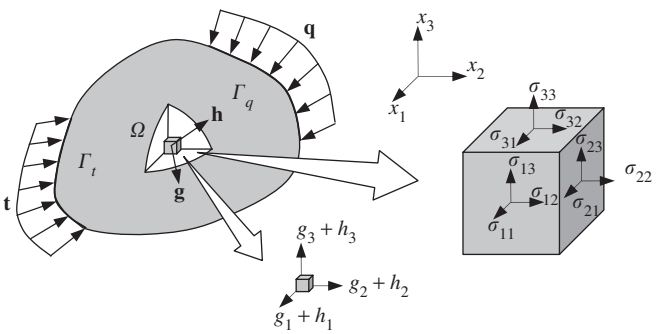

Figure 1. A body subject to a system of surface and body forces.

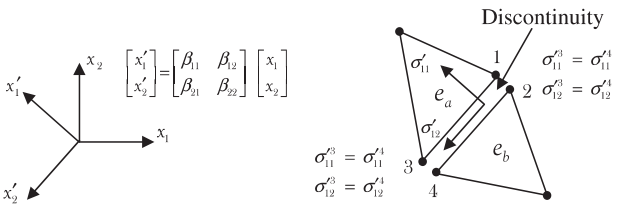

Figure 2. Statically admissible stress discontinuity in 2D.

balances the prescribed tractions $\mathbf{t}$ on Γ_t, nowhere violates the yield criterion, and maximizes the integral

$$Q = \int_{\Gamma_q} \mathbf{q}\, \mathrm{d}\Gamma + \int_{\Omega} \mathbf{h}\, \mathrm{d}\Omega \tag{1}$$

In the present formulation of the lower bound theorem, linear finite elements are used to discretize the continuum. If D is the problem dimensionality, then there are $D+1$ nodes in each element and each node is associated with a $(D^2+D)/2$-dimensional vector of stress variables $\{\sigma_{ij}\}$, $i=1,\ldots,D$; $j=i,\ldots,D$. These stresses, together with the body force components h_i which act on a unit volume of material, are taken as the problem variables. The vector of unknowns for an element e is denoted by $\boldsymbol{\sigma}^e$ and may be written as

$$\boldsymbol{\sigma}^e = \{\{\sigma_{ij}^1\}^{\mathrm{T}}, \ldots, \{\sigma_{ij}^{D+1}\}^{\mathrm{T}}, \{h_i^e\}^{\mathrm{T}}\}^{\mathrm{T}}; \quad i=1,\ldots,D; \quad j=i,\ldots,D \tag{2}$$

With a linear variation of the stresses, a convex yield condition is strictly satisfied throughout an element if it is satisfied at all the element's nodes. Statically admissible stress discontinuities at all inter-element boundaries of the linear elements may be incorporated by imposing additional constraints on the nodal stresses as shown in Figure 2. These discontinuities permit large stress jumps over an infinitesimal distance and reduce the number of elements needed to predict the collapse load accurately. In general, the role of the discontinuities is crucial as their arrangement and distribution has a dramatic influence on the accuracy of the lower bound solution [10].

When the stress field is modelled using linear finite elements, the objective function and equality constraints arising from the equilibrium, boundary, discontinuity, and loading conditions are linear in the unknowns, with the only non-linearity arising from the yield inequalities. Thus the problem of finding a statically admissible stress field which maximizes the collapse load may be stated as

$$\begin{aligned} &\text{maximize} \quad \alpha \\ &\qquad\qquad \mathbf{B}^{\mathrm{T}}\boldsymbol{\sigma} = \alpha\mathbf{p} + \mathbf{p}_0 \\ &\text{subject to} \quad f_j(\boldsymbol{\sigma}) \leqslant 0, \quad j \in J_\sigma \end{aligned} \tag{3}$$

where α is a scalar load parameter, $\mathbf{B}^{\mathrm{T}}$ is an $m \times n$ matrix of equality constraint coefficients, $\mathbf{p}$ and $\mathbf{p}_0$ are vectors of coefficients for optimized and prescribed loads, respectively, $f_j(\boldsymbol{\sigma})$ are yield functions, J_σ is the set of constraints on the stress variables, $\boldsymbol{\sigma}$ is an n-dimensional vector which is to be determined, and n is the number of unknown stresses.

Because the objective function and equality constraints are linear, and the functions f_j are convex, problem (3) is equivalent to the system of Karush–Kuhn–Tucker (KKT) optimality conditions [11, 12]

$$\left.\begin{aligned} &\mathbf{B}^{\mathrm{T}}\boldsymbol{\sigma} = \alpha\mathbf{p} + \mathbf{p}_0 \\ &\mathbf{f}(\boldsymbol{\sigma}) \leqslant \mathbf{0} \end{aligned}\right\} \quad \text{primal-lower bound}$$

$$\left.\begin{aligned} &\mathbf{B}\mathbf{u} - \nabla\mathbf{f}(\boldsymbol{\sigma})\boldsymbol{\lambda} = \mathbf{0} \\ &\mathbf{p}^{\mathrm{T}}\mathbf{u} = 1 \\ &\boldsymbol{\lambda} \geqslant \mathbf{0} \end{aligned}\right\} \quad \text{dual-'upper bound'} \tag{4}$$

$$\left.\begin{aligned} &\boldsymbol{\Lambda}\mathbf{f}(\boldsymbol{\sigma}) = \mathbf{0} \end{aligned}\right\} \quad \text{'plastic consistency'}$$

where $\boldsymbol{\sigma}$ is the optimal solution, $\mathbf{u}$ and $\boldsymbol{\lambda}$ are unknown multipliers, and $\boldsymbol{\Lambda} = \mathrm{diag}(\boldsymbol{\lambda})$. Detailed descriptions of a robust non-linear algorithm for solving the lower bound problem (4) can be found in Lyamin [13] and Lyamin and Sloan [14]. An alternative procedure, which performs well for problems with linear yield conditions, is described in Krabbenhoft and Damkilde [12].

3. ESTIMATION OF THE INTERPOLATION ERROR

It can be shown (see, for example, Almeida *et al.* [15]) that, at some point $\mathbf{x}$ in the vicinity of a point $\mathbf{x}_0$, the difference between a given function $\mathbf{u}$ and its discrete approximation $\mathbf{u}_h$ can be estimated using the following expression:

$$\|\mathbf{u} - \mathbf{u}_h\|_{L^p(\Omega)} \simeq C\|\mathbf{H}_{\mathrm{R}}(\mathbf{u}_h(\mathbf{x}_0))(\mathbf{x} - \mathbf{x}_0) \cdot (\mathbf{x} - \mathbf{x}_0)\|_{L^p(\Omega)} \tag{5}$$

where $\mathbf{H}_{\mathrm{R}}(\mathbf{u}_h(\mathbf{x}_0))$ denotes a recovered Hessian matrix. This demonstrates that the interpolation error is not distributed in an isotropic way around point $\mathbf{x}$, but depends on the vector $(\mathbf{x} - \mathbf{x}_0)$ and the recovered Hessian matrix $\mathbf{H}_{\mathrm{R}}(\mathbf{u}_h(\mathbf{x}_0))$. An anisotropic error estimator for element T of a partition $\mathscr{T}_h$ of Ω has been introduced in [15] as

$$\eta_T = \left\{ \int_{\Omega_T} (\mathbf{G}(\mathbf{u}_h(\mathbf{x}_0))(\mathbf{x} - \mathbf{x}_0) \cdot (\mathbf{x} - \mathbf{x}_0))^p \, \mathrm{d}\Omega \right\}^{1/p} \tag{6}$$

where $\mathbf{G}$ is a positive semi-definite matrix defined by

$$\mathbf{G} = \mathbf{Q}\boldsymbol{\Lambda}\mathbf{Q}^{\mathrm{T}} \tag{7}$$

and $\mathbf{Q}$ is the matrix of eigenvectors of the recovered Hessian matrix with $\boldsymbol{\Lambda} = \mathrm{diag}\{|\lambda_1|, |\lambda_2|, \ldots, |\lambda_D|\}$ being composed of the absolute values of the associated eigenvalues sorted in ascending order $(|\lambda_1| \leqslant |\lambda_2| \leqslant \cdots \leqslant |\lambda_D|)$.

Using (6) and (7), an upper bound for the anisotropic error estimator has been given by Almeida *et al.* [15] as

$$\eta_T \leqslant \left\{ \int_{\Omega_T} \left(\sum_{i=1,D} |\lambda_i(\mathbf{x}_0)| h_i^2 \right)^p \mathrm{d}\Omega \right\}^{1/p} \tag{8}$$

If we require that the estimated error yields the same value in any direction, i.e. $|\lambda_1|h_1^2 = |\lambda_2|h_2^2 = \cdots = |\lambda_D|h_D^2$, we obtain the following error estimator

$$\eta_T = D\Omega_T^{1/p}|\lambda_D(\mathbf{x}_0)|h_D^2 \tag{9}$$

The corresponding global error indicator η is then given by

$$\eta = \left\{ \sum_{T \in \mathscr{T}_h} (\eta_T)^p \right\}^{1/p} \tag{10}$$

and a dimensionless error indicator μ can be introduced as

$$\mu = \frac{\eta}{(\|\mathbf{u}_h\|_{L^p(\Omega)}^p + \eta^p)^{1/p}} \tag{11}$$

4. THE OPTIMAL-MESH-ADAPTIVE SCHEME

Mesh refinement usually proceeds by adjusting the element size to distribute the local error uniformly over the problem domain. An alternative approach is to obtain the element size distribution which minimizes the global error given by (10). This strategy is known as the optimal-mesh-adaptive technique and is described in detail, e.g. by Almeida *et al*. [15]. In our study, we implemented a modified version of what is given in [15] and a brief summary of the procedure is therefore given. The optimal-mesh-adaptive procedure can be cast as a constrained optimization problem which, for the two-dimensional case, becomes

$$\begin{aligned} &\text{minimize} \quad \mathscr{F}(h_{2T}) = \{\eta(h_{2T})\}^p = \sum_{T \in \mathscr{T}_k} \Omega_T |2\lambda_{2T}|^p h_{2T}^{2p} \\ &\text{subject to} \quad N_{\mathscr{T}_{k+1}} = (4/\sqrt{3}) \sum_{T \in \mathscr{T}_k} \Omega_T/(s_T h_{2T}^2) \quad \text{to find } h_{2T}, T \in \mathscr{T}_k \end{aligned} \tag{12}$$

where h_{2T} and s_T are the new size and the stretching of element T, $\mathscr{T}_k$ is the finite element discretization at the adaptation step k, and $N_{\mathscr{T}_{k+1}}$ is the desired number of elements at the step $k+1$.

Introducing the notations

$$C_{1T} = \Omega_T |2\lambda_{2T}|^p, \quad C_{2T} = 4\Omega_T/(\sqrt{3}s_T), \quad \gamma_T = 1/h_{2T}^2 \tag{13}$$

the minimization problem (12) can be rewritten as follows:

$$\begin{aligned} &\text{minimize} \quad \mathscr{F}(\gamma_T) = \sum_{T \in \mathscr{T}_k} C_{1T}/\gamma_T^p \\ &\text{subject to} \quad N_{\mathscr{T}_{k+1}} = \sum_{T \in \mathscr{T}_k} C_{2T}\gamma_T \quad \text{to find } \gamma_T, T \in \mathscr{T}_k \end{aligned} \tag{14}$$

This is equivalent to the following min–max problem

$$\min_{\gamma_T} \max_{\beta} \mathscr{L}(\gamma_T, \beta) = \mathscr{F}(\gamma_T) - \beta \left(N_{\mathscr{T}_{k+1}} - \sum_{T \in \mathscr{T}_k} C_{2T}\gamma_T \right) \tag{15}$$

whose solution given by

$$h_{2T}=\sqrt{1/\gamma_T}=\sqrt{(\beta C_{2T}/pC_{1T})^{1/(p+1)}},\quad \beta^{1/(p+1)}=\frac{1}{N_{\mathscr{T}_{k+1}}}\sum_{T\in\mathscr{T}_k} C_{2T}(pC_{1T}/C_{2T})^{1/(p+1)} \tag{16}$$

Note that setting $s_T=1$ in (12) will result in an optimal mesh size distribution for equilateral elements, while setting λ_T also equal to 1 gives the element size for a uniform mesh with $N_{\mathscr{T}_{k+1}}$ elements.

The optimal-mesh-adaptive procedure described above leads to a curvature-based (or Hessian-based) mesh size distribution in the newly generated grid. However, near the plastic zone, errors can be expected to be based on the gradient of the control variable [5]. Enforcing $h_T\|\nabla_R\mathbf{u}_{h_T}\|=\alpha$ for all elements in the new mesh, we can then write

$$N_{\mathscr{T}_{k+1}}=(4/\sqrt{3})\sum_{T\in\mathscr{T}_k}\Omega_T\|\nabla_R\mathbf{u}_{h_T}\|^2\Big/(s_T\alpha^2) \tag{17}$$

This can be solved for α leading to a gradient-based optimal mesh size distribution of the form

$$h_{2T}=\sqrt{(4/(\sqrt{3}N_{\mathscr{T}_{k+1}}\|\nabla_R\mathbf{u}_{h_T}\|^2))\sum_{T\in\mathscr{T}_k}\Omega_T\|\nabla_R\mathbf{u}_{h_T}\|^2\Big/s_T} \tag{18}$$

5. ADVANCING FRONT MESH GENERATOR FOR LOWER BOUND LIMIT ANALYSIS

The advancing-front-type mesh generator proposed by Peraire *et al*. [1] has proved to be convenient for adaptive remeshing procedures that involve element elongation [8]. It appears that this technique is also ideally suited for generating fans of finite elements—an important feature of lower bound computations when singular points are present in the stress field. Because of the difficulty in controlling the assembly of an optimal unstructured mesh around a singular point, a special (structural) element generation technique can be used in such zones. The rules for internal node placement in the advancing front need to be modified only slightly to produce the required fan of elements at specified points on the initial front. The only additional information needed is the location of the origin for each fan, the density of the elements in the fan, and the threshold distance beyond which we switch to the normal advancing front routine. Some examples of meshes with multiple fan inclusions are shown in Figure 3.

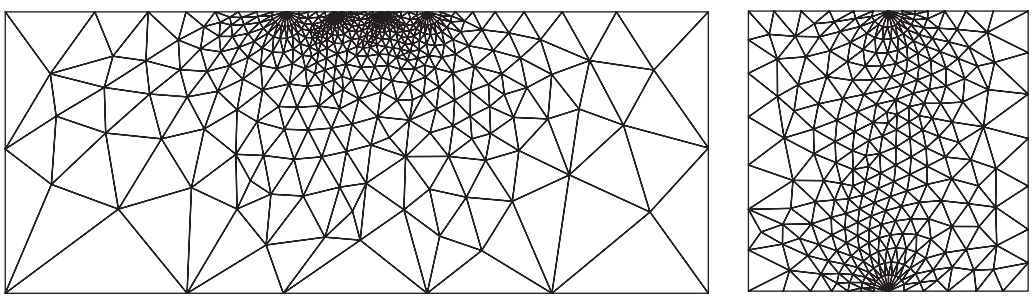

Figure 3. Examples of meshes for problems with multiple singularities in stress field.

6. CHOICE OF CONTROL VARIABLE

The choice of a reliable control variable is not obvious for lower bound limit analysis. What is clear is that the majority of the degrees of freedom must be concentrated in zones of plastic yielding if we are to expect accurate collapse load estimates. As the primary variables are the stresses, one option is to use the yield condition directly to check if a stress point is yielding [6]. However, numerical experience shows that many points which are outside the plastic zone are almost on the yield surface, especially for conical yield criteria. Neither the value of the yield function itself, nor its normalized equivalent (e.g. with respect to the second stress invariant), are representative at such points. Therefore, any criterion that is based on the vicinity of the stress point to the yield surface is unlikely to be a reliable option for adaptive procedure.

Another option for a suitable control variable can be sought from purely mathematical programming considerations. In the optimality conditions (4), the Lagrange multipliers for the inequality constraints directly indicate which inequalities are active and, therefore, which stress points are undergoing plastic flow. Another motivation for using Lagrange multipliers as the control variables can be derived by considering the dual to the lower bound optimization problem which is given by

$$\begin{array}{lll} \text{minimize} & \boldsymbol{\sigma}^{\mathrm{T}}(\nabla \mathbf{f}(\boldsymbol{\sigma})\boldsymbol{\lambda}) - \mathbf{p}_{\mathbf{0}}^{\mathrm{T}}\mathbf{u} & \text{'internal work'} \\ \text{subject to} & \mathbf{B}^{\mathrm{T}}\boldsymbol{\sigma} = \alpha\mathbf{p} + \mathbf{p}_0 & \text{'compatibility'} \\ & \mathbf{p}_0^{\mathrm{T}}\mathbf{u} = 1 & \text{constant 'external work'} \end{array} \tag{19}$$

Here, the interpretation of the quantity

$$\boldsymbol{\sigma}^{\mathrm{T}}(\nabla \mathbf{f}(\boldsymbol{\sigma})\boldsymbol{\lambda}) = \boldsymbol{\sigma}^{\mathrm{T}}\dot{\boldsymbol{\varepsilon}} \tag{20}$$

as the internal dissipation makes sense if

$$\dot{\boldsymbol{\varepsilon}}_j = \lambda_j \nabla f_j(\boldsymbol{\sigma}) \tag{21}$$

are interpreted as the plastic strain rates.

By using the KKT conditions (4) it can be shown that the internal dissipation in (19) is equal to α in (3):

$$\begin{aligned} W^i &= \boldsymbol{\sigma}^{\mathrm{T}}(\nabla \mathbf{f}(\boldsymbol{\sigma})\boldsymbol{\lambda}) - \mathbf{p}_0^{\mathrm{T}}\mathbf{u} \\ &= \boldsymbol{\sigma}^{\mathrm{T}}\mathbf{B}\mathbf{u} - \mathbf{p}_0^{\mathrm{T}}\mathbf{u} \\ &= \mathbf{u}^{\mathrm{T}}(\alpha\mathbf{p} + \mathbf{p}_0) - \mathbf{p}_0^{\mathrm{T}}\mathbf{u} \\ &= \alpha \end{aligned} \tag{22}$$

Thus, the value λ in a given area of the domain is a direct measure of its relative contribution to the load multiplier α.

7. NUMERICAL EXAMPLES

Two classical examples from soil mechanics are considered in this section to judge the efficiency of the adaptive schemes proposed. The first example, the stability of a vertical cut in a purely cohesive soil, represents a class of problems where no strong singularities are present in the stress boundary conditions. The second example, a rigid strip footing on a cohesive-frictional soil is, on the contrary, a case where such a singularity is highly pronounced. This fact, as it will be shown later, requires a special mesh pattern (fan) to be constructed around the singular point in order to obtain results of optimal accuracy.

The range of adaptive schemes which have been tested on the above-mentioned stability problems can be listed as follows:

1. Uniform mesh.
2. Uniform mesh + fan.
3. L value-based optimal mesh.
4. L gradient-based optimal mesh.
5. L Hessian-based optimal mesh.
6. L Hessian-based optimal mesh + fan.
7. L Hessian-based optimal mesh + anisotropy.
8. L Hessian-based optimal mesh + anisotropy + fan.

The symbol L is used here, and in the following sections, to denote Lagrange multipliers in figures and graphs.

7.1. Critical height of an unsupported vertical cut

The stability of a vertical cut in a purely cohesive soil is governed by the dimensionless parameter (stability number) $N_s = \gamma H/c$, which implies that the vertical body force (unit weight) can be optimized for a given cohesion and cut height. The initial mesh used to start the adaptivity process is shown in Figure 4, together with the stress boundary conditions. Although the exact solution remains unknown, very tight bounds have been recently reported [14] ($3.772 \leqslant N_s \leqslant 3.782$) [16]. Therefore, the accuracy of the obtained results can be verified easily.

As no stress singularities are present in the stress boundary conditions for this problem, only four adaptive schemes (with no fan option) have been tested here with the results plotted in Figure 4. It is clearly seen from this figure that the anisotropic mesh refinement approach (scheme 7) performs worse than schemes 3–5 where equilateral finite elements are employed. This is in contrast to the results reported by Borges *et al.* [8] for mixed limit analysis formulations, where the velocities are the primary variables and elongation of the elements along slip bands is advantageous. In the case of lower bound limit analysis, stretching the elements along plastic bands can have a negative effect when this direction is close to the direction of stress field gradient. This is because the density of degrees of freedom is reduced in the direction of the maximum variation of stresses, leading to a less accurate solution.

On the other hand, employing the stresses as control variables (with the aim of elongating the elements along stress field isolines) does not give better results either, as the stress field distribution does not reflect the plastic localization zones where the major concentration of degrees of freedom is needed (Figure 5). These observations speak for choosing the plastic multiplier as the control variable, together with equilateral finite elements, as the most reliable

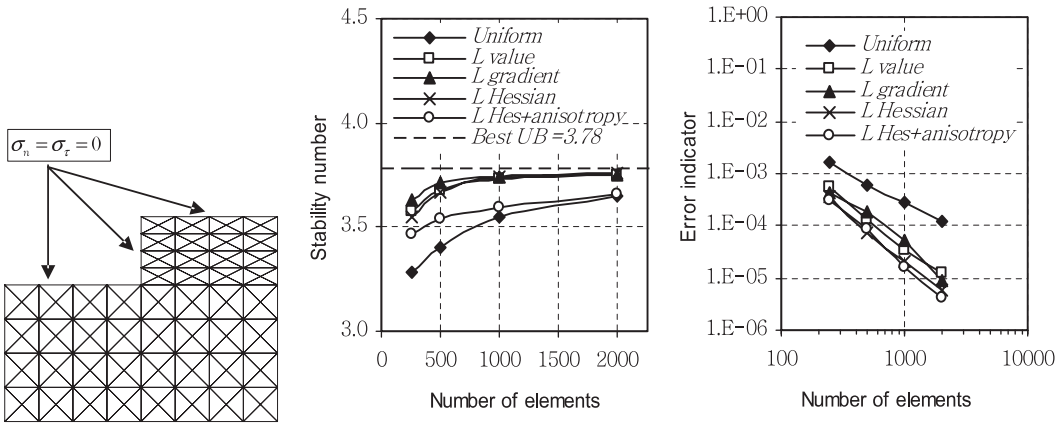

Figure 4. Vertical cut initial mesh and adaptive schemes performance comparison.

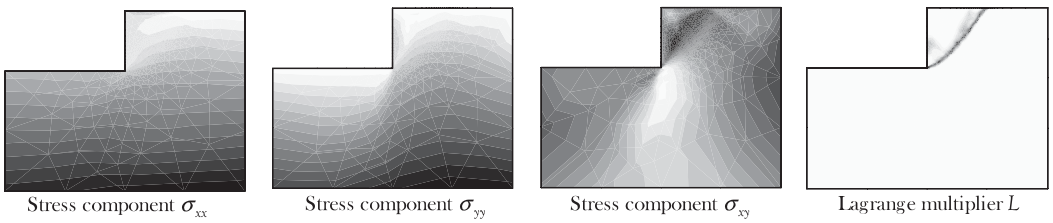

Figure 5. Stress field and plastic multiplier distribution for vertical cut problem.

option for adaptive lower bound limit analysis when there are no stress singularities in the stress boundary conditions.

All adaptivity schemes with isotropic mesh refinement demonstrate similar performance, achieving better than 1 per cent accuracy for a mesh of 2000 elements. The meshes generated using uniform refinement, L Hessian-based refinement, and L Hessian-based refinement and anisotropy are shown in Figure 6 and the corresponding stability numbers are summarized in Table I. It should be noted that the best-known lower bound of 3.772 was obtained using a specially arranged mesh containing more than 6000 elements [14].

The other way to compare the efficiency of competing approaches is the static adaptivity test, where all subsequent computations are performed maintaining a constant number of elements in the mesh. The results of such a test with 2000 elements, plotted in Figure 7, suggest that the L Hessian- and L value-based adaptive schemes are slightly better performers than the L gradient-based scheme.

For all the static adaptivity schemes considered, a near-optimal mesh pattern is achieved after 3–4 iterations and the corresponding limit loads are very similar to those from the 2000 element meshes obtained by increasing the number of elements. Note that continued remeshing with a constant number of elements does give some small fluctuations in the results due to mesh generation imperfections.

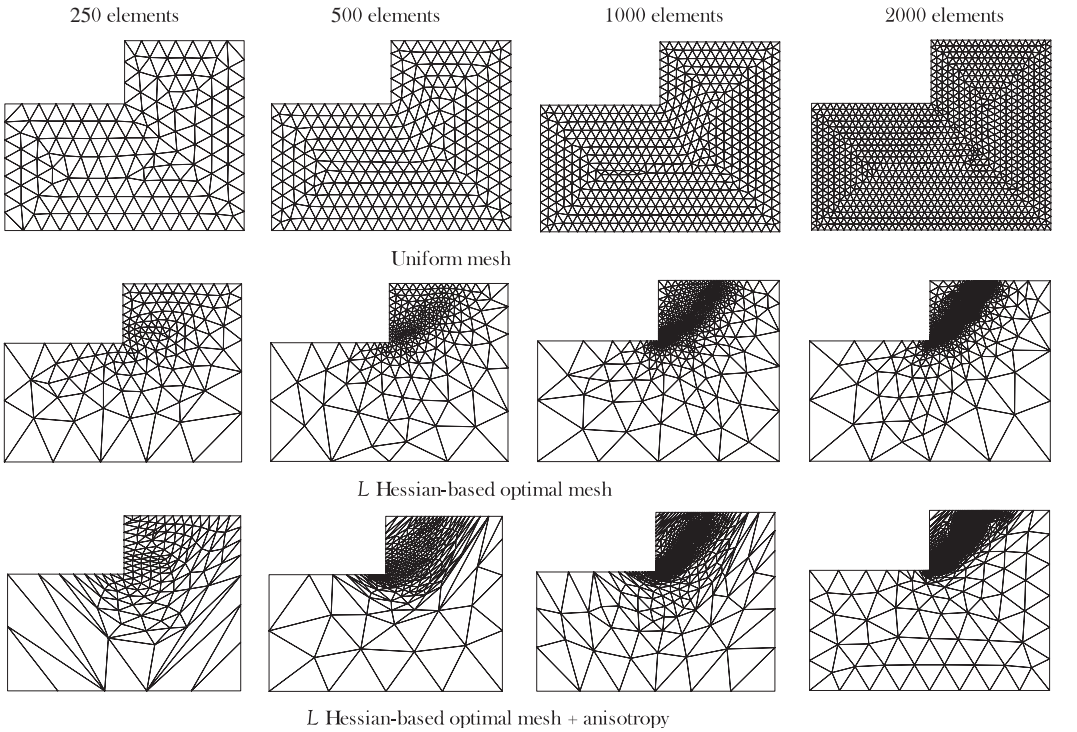

Figure 6. Mesh adaptation progress using different adaptive schemes for vertical cut problem.

Table I. Efficiency of different adaptive strategies for vertical cut problem ($c = 1$, $\phi = 0°$).

	Collapse load			
Adaptive strategy	250 elements	500 elements	1000 elements	2000 elements
1. Uniform	3.28	3.40	3.55	3.65
3. L value	3.57	3.68	3.74	3.75
4. L gradient	3.63	3.71	3.74	3.75
5. L Hessian	3.55	3.67	3.74	3.76
7. L Hessian + anisotropy	3.47	3.54	3.59	3.66

7.2. Rigid smooth strip footing on cohesive-frictional soil

For a rigid strip footing on a weightless cohesive-frictional soil with no surcharge, the exact collapse pressure is given by the Prandtl [17] solution

$$q/c' = (\mathrm{e}^{\pi \tan \phi'} \tan^2(45 + \phi'/2) - 1) \cot \phi' \tag{23}$$

where c' and ϕ' are, respectively, the effective cohesion and the effective friction angle. For a soil with a friction angle of 30° this equation gives $q/c' = 30.15$. The stress boundary conditions used in the analysis, together with the initial mesh, are shown in Figure 8.

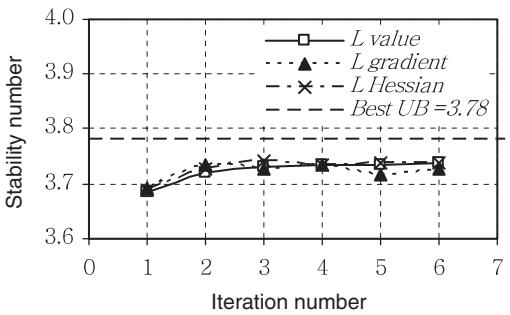

Figure 7. Static adaptivity test for vertical cut problem (2000 elements).

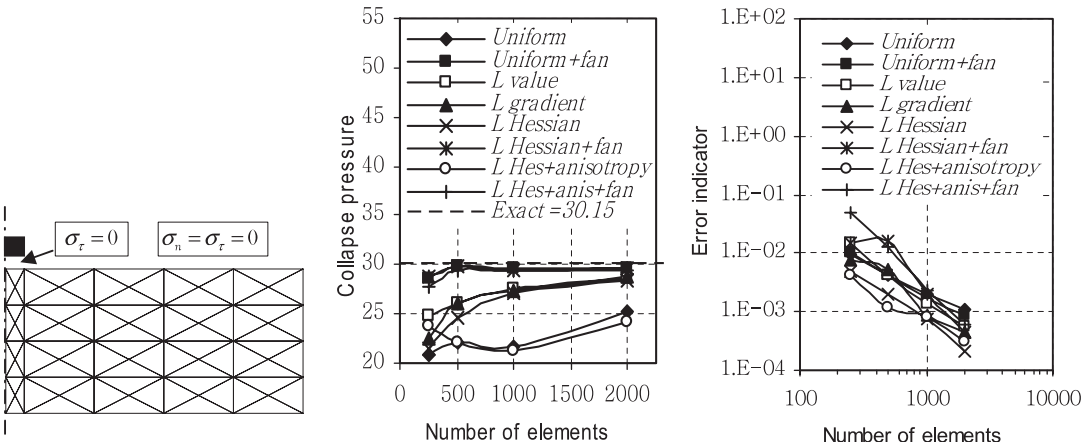

Figure 8. Strip footing initial mesh and adaptive schemes performance comparison.

The graphs presented in Figure 8 demonstrate the performance of each of the adaptive approaches described earlier. The meshes used for the strip footing problem are shown in Figure 9. It is clear that the accuracy of the analysis is now much more dependent on the number of discontinuities originating from the stress singularity at the footing edge, rather than on the element size distribution over the problem domain. Even a uniform mesh with a moderate number of elements gives quite accurate solutions, provided there is a sufficient number of wedge elements (with discontinuities between them) in the fan centred on the footing edge (see Figure 8, Table II). This behaviour is explained in detail by Chen [10], who shows that a fan of discontinuities allows for rapid rotations of the principal stresses by means of consecutive jumps in the tangential stress components across each discontinuity. Larger numbers of discontinuities give larger principal stress rotations which, in turn, give bigger differences in the vertical stresses on opposite sides of the singular point. This suggests that the mesh around a singular point should be governed by a fan-like stress field (see Figure 10), with the density of elements in the fan being governed by the magnitude of the stress gradients in the radial and circumferential directions. Although promising, this option has yet to be implemented, and only a uniform fan is automatically constructed where appropriate.

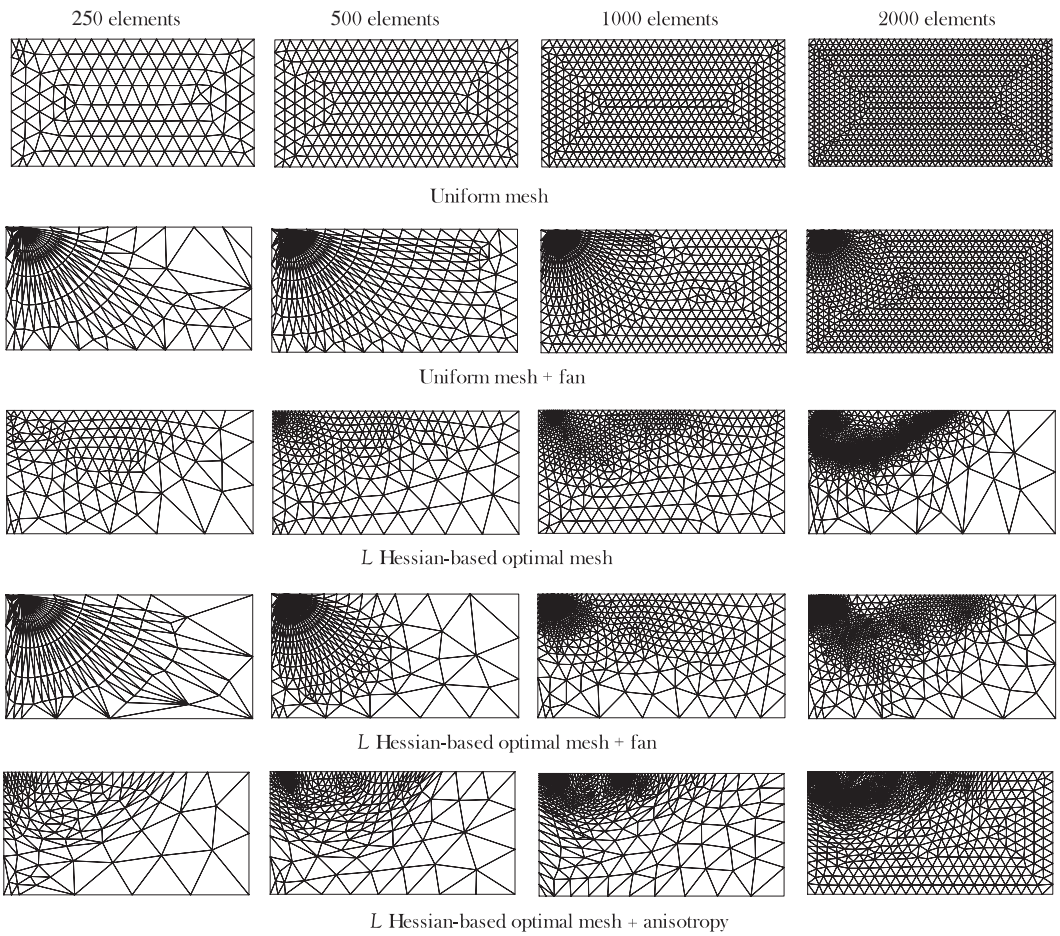

Figure 9. Mesh adaptation progress using different adaptive schemes for strip footing problem.

Table II. Efficiency of different adaptive strategies for strip footing problem ($c' = 1$, $\phi' = 30°$).

	Collapse load			
Adaptive strategy	250 elements	500 elements	1000 elements	2000 elements
1. Uniform	20.77	22.10	21.73	25.27
2. Uniform + fan	28.66	29.76	29.61	29.60
3. *L* value	24.78	26.06	27.57	28.68
4. *L* gradient	22.46	25.98	27.42	28.88
5. *L* Hessian	21.57	24.55	27.10	28.43
6. *L* Hessian + fan	28.72	29.86	29.43	29.58
7. *L* Hessian + anisotropy	23.73	22.10	21.17	24.14
8. *L* Hessian + anisotropy + fan	27.82	29.42	29.45	29.40

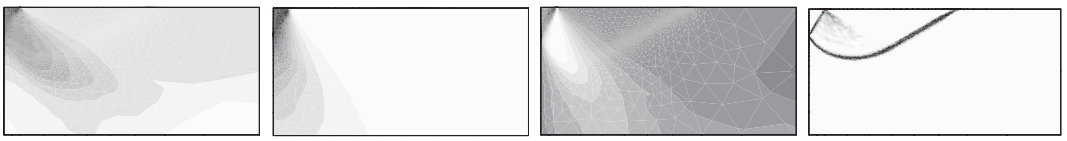

Figure 10. Stress field and plastic multiplier distribution for strip footing problem.

Apart from this feature a number of possible adaptive schemes for lower bound limit analysis have been tested, and the results obtained seem to suggest the following approach. The stress field obtained from an initial (or previous) mesh is analysed to check for the existence of singular points. If such points are detected, then the error estimation and element size distribution around them are governed by the stress field behaviour. Elsewhere, the mesh assembly should be controlled using the plastic multiplier field with no element stretching.

8. CONCLUSIONS

Different adaptive schemes have been tested for lower bound limit analysis. The results obtained show that an optimal-mesh-adaptive procedure, based on the magnitude of the Lagrange multipliers, appears to be the most suitable option for lower bound computations (particularly when coupled with an automatic generation of 'fan' zones at singular points in the stress field). For both numerical examples considered in the study, the adaptive scheme was able to predict the actual collapse load with less than 1 per cent error with a moderate number of elements in the mesh.

REFERENCES

1. Peraire J, Vahdati M, Morgan K, Zienkiewicz OC. Adaptive remeshing for compressible flow computations. *Journal of Computational Physics* 1987; **72**:449–466.
2. Zienkiewicz OC, Huang M, Pastor M. Localization problems in plasticity using finite elements with adaptive remeshing. *International Journal for Numerical and Analytical Methods in Geomechanics* 1995; **19**:127–148.
3. Löhner R. Adaptive remeshing for transient problems. *Computer Methods in Applied Mechanics and Engineering* 1989; **75**:195–214.
4. Lo SH, Lee CK. Solving crack problems by an adaptive refinement procedure. *Engineering Fracture Mechanics* 1992; **43**:147–163.
5. Jonson C, Hansbo P. Adaptive finite element methods in computational mechanics. *Computer Methods in Applied Mechanics and Engineering* 1992; **101**:143–181.
6. Christiansen E, Pedersen OS. Adaptive mesh refinement in limit analysis. *International Journal for Numerical Methods in Engineering* 2001; **50**:1331–1346.
7. Murthy KSRK, Mukhopadhyay M. Adaptive finite element analysis of mixed-mode crack problems with automatic mesh generator. *International Journal for Numerical Methods in Engineering* 2000; **49**:1087–1100.
8. Borges LA, Zouain N, Costa C, Feijóo R. An adaptive approach to limit analysis. *International Journal of Solids and Structures* 2001; **38**:1707–1720.
9. Lyamin AV, Sloan SW. Mesh generation for lower bound limit analysis. *Advances in Engineering Software* 2003; **34**:321–338.
10. Chen WF. *Limit Analysis and Soil Plasticity*. Elsevier: Amsterdam, 1975.
11. Nash SG, Sofer A. *Linear and Nonlinear Programming*. McGraw-Hill: New York, 1996.

12. Krabbenhoft K, Damkilde L. A general non-linear optimization algorithm for lower bound limit analysis. *International Journal for Numerical Methods in Engineering* 2003; **56**:165–184.
13. Lyamin AV. Three-dimensional lower bound limit analysis using nonlinear programming. *Ph.D. Thesis*, Department of Civil, Surveying and Environmental Engineering, University of Newcastle, NSW, 1999.
14. Lyamin AV, Sloan SW. Lower bound limit analysis using nonlinear programming. *International Journal for Numerical Methods in Engineering* 2002; **55**:573–611.
15. Almeida RC, Feijóo R, Gleão AC, Padra C, Silva RS. Adaptive finite element computational fluid dynamics using an anisotropic error estimator. *Computer Methods in Applied Mechanics and Engineering* 2000; **182**: 379–400.
16. Pastor J, Thai TH, Francescato P. New bounds for the height limit of a vertical slope. *International Journal for Numerical and Analytical Methods in Geomechanics* 2000; **24**:165–182.
17. Prandtl L. Über die Härte plastischer Körper. Göttingen. *Nachrichten Mathematisch-Physikalishe Klasse* 1920; **12**:74–85.

